Plasma channel flows: Electro-fluid dynamic jets

Nicholas S. Campbell and Subrata Roy
Applied Physics Research Group, Department of Mechanical and Aerospace Engineering, University of Florida, Gainesville, Florida 32611, USA

(Received 3 September 2014; accepted 24 September 2014; published online 2 October 2014)

The present work builds on the success of a dielectric barrier discharge driven plasma channel by exploring an electrode configuration that directly actuates the bulk fluid minimizing jet impingement and viscosity related losses. Influence of several electrical and physical parameters including electrode materials are experimentally investigated. Results indicate significant variation of performance with these parameters and suggest that in comparison to surface dielectric barrier plasma actuator driven flows, at least an order of magnitude improvement in efficiency is possible. The jet produced from this plasma channel configuration allows greater versatility for applications in boundary layer flow control and internal flows. © *2014 AIP Publishing LLC*.
[http://dx.doi.org/10.1063/1.4897341]

Recently, the concept of a surface dielectric barrier discharge (SDBD) driven channel flow has been introduced.[1] In this arrangement, each surface mounted plasma actuator creates its own semi-bounded wall jet, which is confined to a channel coalesces downstream to form a plug flow like velocity profile at the outlet. The average outlet velocity of this channel is found to be a function of number of actuators as well as the applied voltage (for a given geometry).[2,3] The classical SDBD is known to induce a suction effect upstream of the surface compliant exposed electrode. The majority flow in this suction is normal to the surface, which upon impingement on the wall changes its direction and subject to the plasma injected body force generates a very thin Glauart-like wall jet parallel to the surface. This process is quite energy inefficient. Bounding the actuator in a channel ensures the majority flow to be axial and hence allows better conservation of the upstream kinetic energy of the flow. However, the energy conversion efficiency for the SDBD based plasma channel remains low approaching 0.1%,[3] which is similar to that of the traditional surface mounted linear actuator. This is due to excessive viscous loss from the thin wall shear layer of the traditional linear SDBD actuator configuration.[4]

In this letter, an actuator configuration has been developed that aims to mitigate high viscous losses due to the local momentum injection near a solid surface and to demonstrate improvement thereof in electro-fluid mechanical efficiencies.

Reported experiments show[5,6] that an SDBD using micron size wire and insulated plate resulted in decreased streamers and thus better flow performance than the standard plate-to-insulated plate electrode configuration. For example, using a horizontal gap of 5 mm between the wire and encapsulated plate electrode, a four staged serial array of these surface mounted actuators[5] produced a velocity peak of 10.5 m/s.

Motivated by the increased performance of a wire electrode, we reconfigured the traditional actuator design by moving the wire far above the surface. For a channel this means symmetric actuators sharing a common wire in middle. Such electrode arrangement should allow direct momentum injection into the bulk flow being comparatively less affected by wall shear than its traditional counterpart. Figure 1 presents the channel geometry along with the electrode configuration. The channel inside is l_{ch} long, h_{ch} high, and w_{ch} wide (spanwise width, normal to the plane of the paper). A wire of diameter d is kept upstream of an encapsulated plate electrode of width w and thickness t_{ge}. The horizontal distance between the center of the wire to the middle of the plate electrode is g. Half of the channel height ($h_{ch}/2$) represents the vertical distance between the center of the exposed wire electrode to mid location of the plate electrode (see Figure 1(a)). The wire is powered with a kilovolt ac supply and the plate electrodes are grounded. The thickness of the dielectric wall, t_d, is creating a barrier between the plate electrode and the air inside the channel. Hereafter, the jet jutting out at the exit plane of this channel will be referred to as the electro fluid dynamic (EFD) jet.

Multiple revisions of the channel design are used. All channels are of $l_{ch} \times h_{ch} = 40\,\text{mm} \times 5\,\text{mm}$. However, various design revisions differed in length of the spanwise direction and material properties. The channels used to obtain the data presented here are referred to A and D with $w = 100\,\text{mm}$ and 120 mm, respectively. All experiments consisted of a 70 μm thick (t_{ge}) by 12.7 mm wide (w) copper tape that was fully encapsulated inside both top and bottom of the channel dielectric with $t_d = 2\,\text{mm}$ and $g = 5\,\text{mm}$. The acrylic channels are built from a 3D SolidWorks model via Rhinoceros 3D design software, to a 50 W CO_2 laser cutter in the University of Florida Arts and Architecture Fabrication Lab.

A LABView code was utilized to download peak-to-peak voltage and current measurements from a Tektronix DPO2014 oscilloscope. This model has a maximum sampling rate of 1 GSa/s at a bandwidth of 100 MHz. Voltage was measured using a Tektronix (Model P6015A) passive probe having an attenuation of 1000×. The frequency response of the probe is able to measure AC voltages up to 40 kV with a rated accuracy within ±3%. The voltages used in the current study ranged from 10 kV_{pp} to 32 kV_{pp} (5–16 kV amplitudes). Current was measured with a Pearson Electronic's (Model 2100) inductive coil type current probe, also known as a Rogoswki coil. This probe had a manufacturer rated accuracy within ±1% and a 20 MHz bandwidth. The probe outputs a voltage signal that scales as (1 V):(1 A). A sinusoidal output

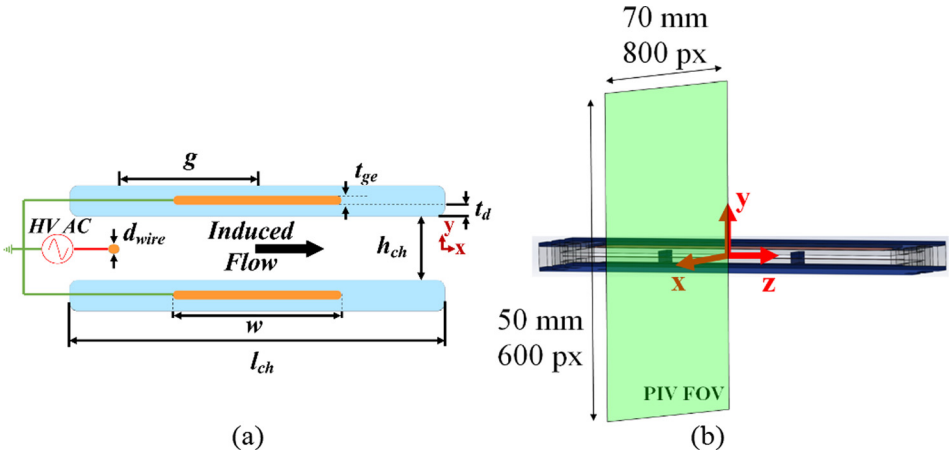

FIG. 1. (a) 2D representation of channel with important length scales and basic powering scheme. (b) Solid model channel with PIV Field of View (FOV).

signal was created in a Tektronix arbitrary function generator (Model AFG3022B), then passed through a QSC audio amplifier (Model RMX 2450) then finally stepped up again through a custom high voltage transformer. Average power consumption was calculated using the V-I method, $P_{elec} = \frac{1}{N}\sum_{i-1}^{N} V_i I_i$, where V_i and I_i are discrete samples of the voltage and current measured, respectively, and N is the number of samples taken. Further details on power measurement methods and their limitations can be found in Durscher.[7] Error in the power measurements is calculated (neglecting temporal error) using $P_{error} = P_{elec}\sqrt{\zeta_V^2 + \zeta_I^2}$, where ζ_V and ζ_I are the voltage and current probe inaccuracies, respectively.

Velocity data are collected on a plane as shown in Figure 1(b) employing the LaVision PIV system with a 532 nm Nd:YAG (New Wave Research Model Solo PIV II 30) fitted with a divergent cylindrical lens to create a laser sheet which illuminates Ondina oil particles. Images are captured by a Phantom 7.3 high speed camera which has a 600 × 800 pixel resolution (represented in Figure 1(b)). These are controlled in LaVision's Davis 7.2 software via Model PTU-9, programmable timing unit (synchronization resolution of 10 ns with <1 ns jitter). Statistical convergence and error estimation in the PIV measurements were considered using the methodology of Durscher.[7] Statistical convergence is found within <300 samples (image pairs); however, 600 samples were taken to ensure adequate data for analysis.

The energy conversion efficiency is defined as the ratio of the fluid mechanical power output to the electrical power input at the load. The fluid mechanical power is based on the velocity information,[8] $P_{mech} = \frac{w_{ch}}{2}\rho\int\int u_x^3 dy$. Note that the aspect ratios (w_{ch}/h_{ch}) for channels A and D are 20 and 24, respectively, for which the end effects are localized near the vertical walls and are minimal (results collected but not shown for brevity). Hence, the flow is essentially two-dimensional and calculating P_{mech} using u_x is assumed a sufficient approximation.

The powered electrode in all baseline test is a 32 AWG ($d_{wire} = 0.2032$ mm) copper wire. Baseline tests are focused on investigating the effect of frequency and applied voltage on the energy conversion efficiency, $\eta = P_{mech}/P_{elec}$. Just as with classical dc and SDBD devices, the both P_{mech} and P_{elec} increase with increasing voltage at constant frequency. However, the specific variation of electrical power (and thus induced velocity) with frequency is based on inherent characteristics of the high voltage circuit being used.[6] A specific transformer powering a given electrode (load) will have a uniquely peaked resonance curve. Two different transformers are used for a desired frequency—one in the range of 0.9–5 kHz and the other between 6 and 30 kHz.

Figure 2 displays PIV data for the velocity field induced by channel A operated with 26 kV_{pp} at 14 kHz. This was the highest applied voltage at the highest frequency tested and thus shows the highest induced velocity of 7.2 m/s in the core. Unlike the surface mounted actuators which have a very small localized high velocity region, the jet shown in Figure 2 has a potential core nearly the same height as the channel (approaching the ideal plug flow profile) while also penetrating the quiescent surroundings around 30 mm from the channels exit before significant dissipation is seen to distribute the momentum vertically. Also, note that this velocity is generated from a single actuator. These qualities suggest that EFD jets may be more advantageous in flow control and propulsion applications as compared to surface mounted actuators.

Figure 3(a) shows the consumed power as a function of applied voltage, for the four different frequencies investigated using two channels A and D. Power fits are used on each data set and collectively show variations ranging from

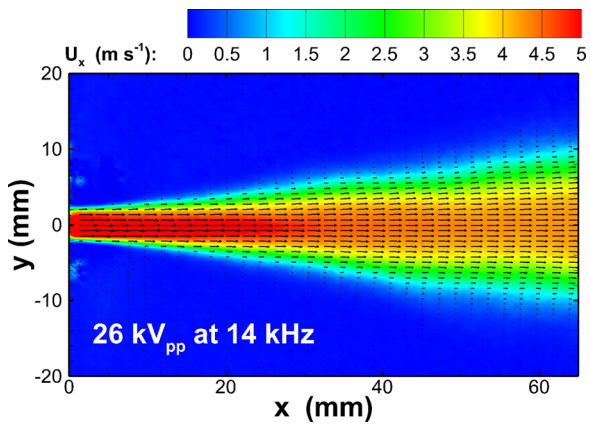

FIG. 2. PIV data for the velocity distribution downstream of the channel A along the x-y plane. The channel was operated with 26 kV_{pp} at 14 kHz. The maximum velocity in red is 7.2 m/s.

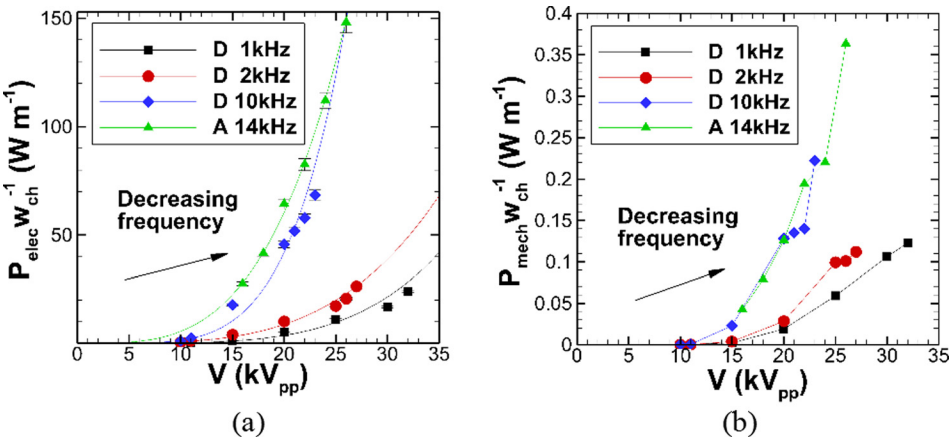

FIG. 3. Performance markers measured for various applied voltages at 4 different operating frequencies for plasma channels A and D. (a) Electrical power consumed by the plasma channel for various applied voltages at 4 different frequencies. (b) Fluid mechanical power generated.

powers of 3 to 5. Similar to other electro-fluidic actuators, power consumption increases with increasing applied voltage at constant frequency and increases with increasing frequency at constant voltage. The arrow in Figure 3(a) denotes the direction of decreasing frequency. At lower frequencies, higher applied voltages can be implemented before small increases in voltage represent prohibitively large increases in consumed power as is seen above 20 kVpp for the two higher frequencies displayed.

Figure 3(b) presents the variation of the fluid mechanical power in the jet produced from the plasma channel. Similar to the variation of consumed power, the data show increased power output for increasing voltage at constant frequency and for increasing frequency at constant voltage. Even though at the higher voltages tested for each frequency, the plasma had transitioned to a streamer regime (as noted visually and audibly), induced fluid mechanical power does not saturate within the range of voltage and frequency investigated. This is, however, not the case for the energy conversion efficiency η, which shows a trend of saturation as plotted in Figure 4. Interestingly, a lower operating frequency extracts higher energy conversion efficiency. Thus for a given voltage, a lower operating frequency will allow a higher percentage of the electrical energy supplied to the powered electrode to actuate the otherwise quiescent fluid in the channel.

These efficiency curves are promising for a number of reasons. First, we see using the assumed channel dimension, specifically an electrode spacing of 5 mm (horizontally), will achieve the level of efficiencies only seen in the multistaged, electrostatic (DC limit) point-to-plane type plasma channels. Noting that efficiency increases with decreasing frequency at constant voltage, this may suggest that simply by operating at even lower frequencies, with these wire-to-insulated plate type plasma channels, that efficiencies on the order of 1% are possible, for the current electrode spacing.

For investigating the influence of electrode spacing, a non-dimensional gap Δ is defined: $\Delta = 2g/w$. For the baseline ($g = 5$ mm), $\Delta = 1.79$. Figure 5 plots the energy conversion efficiency for the channel D with Cu electrode ($d_{wire} = 0.2032$ mm) powered with four different voltages at 4 kHz operating frequency as a function of Δ. For the range of voltages used, the power consumption ($P_{elec}(\Delta)$, not shown for brevity) changes slope around $\Delta = 1.5$. However, for the range of voltages used, a maximum efficiency at converting electrical power to fluid mechanical power production is seen at $\Delta = 1.25$. At some saturation voltage for a given frequency, further increase in applied voltage no longer yields any increase in efficiency. Interestingly, beyond $\Delta = 1.5$ saturation increases as the powered electrode is moved outward. This is certainly a highly nonlinear characteristic of electro-fluidic actuators.

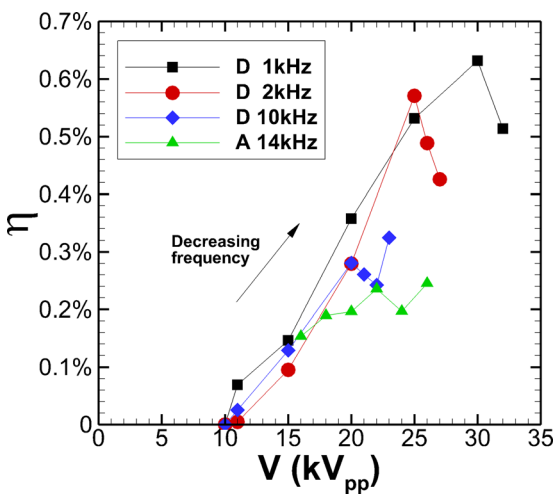

FIG. 4. Efficiency of the plasma channels A and D for various applied voltages and frequencies.

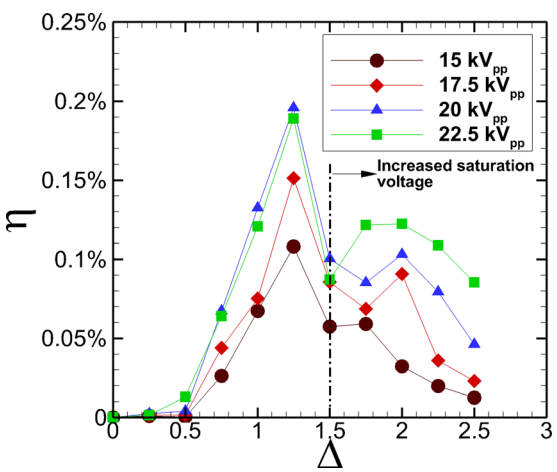

FIG. 5. Effect of electrode spacing on: Energy conversion efficiency of the plasma channel D as a function of electrode spacing Δ at 4 kHz.

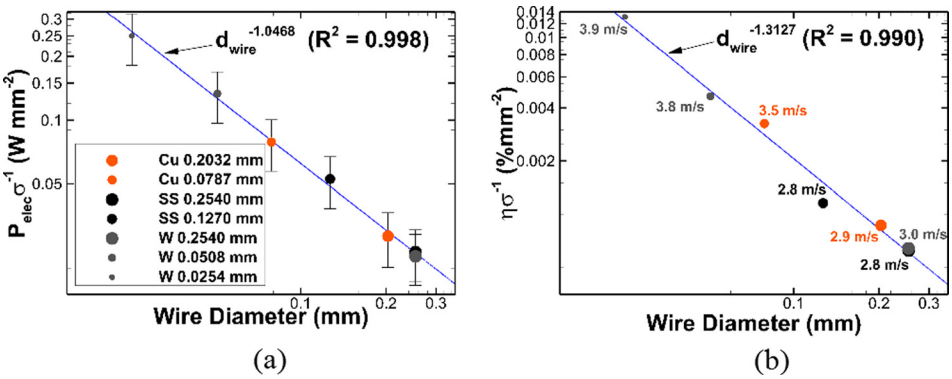

FIG. 6. (a) Consumed electrical power and (b) fluid mechanical efficiency as a function of the powered electrodes effective radius for all electrodes tested. Both (a) and (b) are normalized with electrode surface area, σ. All for the channel D for 20 kV_{pp} at 4 kHz for a gap of $\Delta = 1.00$.

Finally, the effect of size and material of the powered electrode is plotted in Figure 6. These tests are done maintaining $\Delta = 1.0$. Three metals are chosen, copper, stainless steel, and tungsten with varying d_{wire}. Both power consumed (Figure 6(a)) and energy conversion efficiency (Figure 6(b)) are normalized by the wire surface area $\sigma = \pi\, d_{wire}\, w_{ch}$. As expected, much stronger jets are seen for decreasing d_{wire}. In some cases, the high velocity core penetrated upwards of 40 mm from the channels exit into the initially quiescent surrounding fluid, for the smaller tungsten wires. All plots line up nicely, shown by a power fit varying as $d_{wire}{}^{-z}$. For P_{elec}, $z = 1.05$ and for η, $z = 1.31$.

Also shown in Figure 6(b), are the maximum induced velocities measured with PIV for each electrode. Stainless steel does not show an increase in maximum velocity with decreased electrode wire diameter, however, the power consumption and efficiency are seen to increase with such. This is due to the size of the EFD jet potential core. While the maximum induced velocity does not significantly increase, the thickness of the potential core is larger, for the smaller electrode due to larger momentum injection, approaching the ideal plug-flow like velocity profile thus with more mechanical power output relative to the increase in consumed electrical power, the efficiency does increase. Clearly, the stainless steel is the least ideal electrode material tested, as well as the one with the highest resistivity (lowest conductivity) by an order of magnitude. Furthermore, the tungsten's higher tensile strength and only slightly higher resistivity, as compared to copper, makes it a very suitable material for plasma channels. This has been the conclusion for other electrode designs such as in the light bulb and welding industries.

In summary, the performance characterization of a plasma channel with a central wire has been reported. The channel will be suitable candidate for applications in boundary-layer flow control and as a driver for internal gas flows. What makes this plasma channel different is the electrode configuration, high voltage wire-to-encapsulated grounded plate, operating at high alternating frequency. This electrode configuration injects momentum directly into the bulk fluid of the channel with less viscous penalty than a near wall plasma induced jet. This also minimizes wall normal to wall parallel momentum loss which affects the traditional actuator performance. Utilizing an ac signal and dielectric barrier between electrodes to both decrease the needed breakdown voltage amplitude and allow for an extended range of operation and thus enhanced throttleability as a propulsive device. In particular, the strong EFD jet from a single actuator produced high velocity cores (over 5 m/s with 7.2 m/s peak), nearly as thick as the channels height of 5 mm penetrating several centimeters downstream of the channel. The efficiency of such arrangement in converting electrical to fluid kinetic energy can reach up to 700% (0.7% in place of 0.1%) of the standard DBD actuator and channel. The influence of the circular wire material and size was also reported and shown to have an exponential correlation with the performance characteristics of the channel. Based on the data reported, an optimal design of this plasma channel deemed plausible to generate high (10 m/s) jet velocity with practical energy conversion efficiency (>1%) neither of which currently available. Furthermore, study has been undertaken to investigate the role of electrode geometry, using tungsten electrodes and will be presented in future works.

[1]C.-C. Wang and S. Roy, J. Phys. D: Appl. Phys. **42**, 185206 (2009).
[2]M. Debiasi and Li Jiun-Ming, in Proceedings of the 49th AIAA Aerospace Sciences Meeting, Orlando, 2011.
[3]M. Riherd and S. Roy, J. Appl. Phys. **112**, 053303 (2012).
[4]J. Kriegseis, A. Duchmann, C. Tropea, and S. Grundmann, J. Appl. Phys. **114**, 053301 (2013).
[5]A. Debien, N. Benard, and E. Moreau, J. Phys. D: Appl. Phys. **45**, 215201 (2012).
[6]C. Enloe, T. E. McLaughlin, R. D. van Dyken, K. D. Kachner, E. J. Jumper, T. C. Corke, M. Post, and O. Haddad, AIAA J. **42**(3), 595–604 (2004).
[7]R. Durscher, Ph.D. dissertation, University of Florida, 2013.
[8]J. Jolibois and E. Moreau, IEEE Trans. Dielectr. Electr. Insul. **16**(3), 758–767 (2009).